

# Journal Pre-proofs

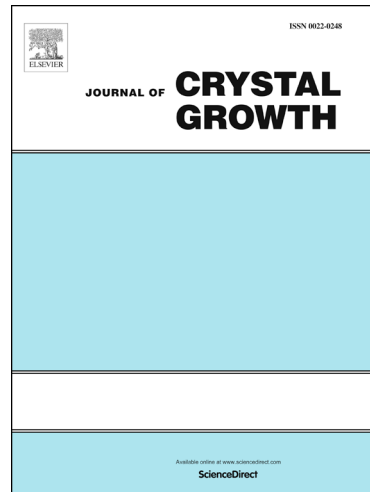
Crystal growth, structure, mechanical, thermal, spectral and optical properties of organometallic of L – Proline Strontium Bromide Tetrahydrate single crystal for nonlinear optical applications

S. Sathiskumar

PII: S0022-0248(19)30449-X

DOI: <https://doi.org/10.1016/j.jcrysgro.2019.125234>

Reference: CRYSG 125234



To appear in: *Journal of Crystal Growth*

Received Date: 26 April 2019

Accepted Date: 10 September 2019

Please cite this article as: S. Sathiskumar, Crystal growth, structure, mechanical, thermal, spectral and optical properties of organometallic of L – Proline Strontium Bromide Tetrahydrate single crystal for nonlinear optical applications, *Journal of Crystal Growth* (2019), doi: <https://doi.org/10.1016/j.jcrysgro.2019.125234>

This is a PDF file of an article that has undergone enhancements after acceptance, such as the addition of a cover page and metadata, and formatting for readability, but it is not yet the definitive version of record. This version will undergo additional copyediting, typesetting and review before it is published in its final form, but we are providing this version to give early visibility of the article. Please note that, during the production process, errors may be discovered which could affect the content, and all legal disclaimers that apply to the journal pertain.

© 2019 Published by Elsevier B.V.

**Crystal growth, structure, mechanical, thermal, spectral and optical properties of organometallic of L – Proline Strontium Bromide Tetrahydrate single crystal for nonlinear optical applications**

**S. Sathiskumar <sup>a,\*</sup>**

<sup>a</sup> Crystal Growth Laboratory, Department of Physics, Shri Angalamman College of Engineering and Technology, Siruganur, Tiruchirappalli – 620 105, Tamil Nadu, India.

---

**Abstract**

Growth of organometallic nonlinear optical (NLO) L – Proline strontium bromide tetrahydrate (LPSBT) single crystals were reported for the first time by slow evaporation technique. Crystal structure was elucidated by single crystal X – ray diffraction analysis. Fourier transform infrared and FT - Raman spectroscopic studies were performed to indentify the various functional groups present in the grown crystal. Optical transmittance of the grown crystal was investigated by UV – Vis – NIR spectral studies. The lower cut off wavelength of the grown crystal is observed at 240 nm. The photoluminescence spectral study of the grown crystal showed an emission peak at 410 nm. Mechanical strength was assessed by Vickers microhardness measurements. The dielectric constant and dielectric loss were studied as a function of frequency at various temperatures. Thermal stability of the grown crystals was studied by thermogravimetric analysis, differential thermal analysis and differential scanning calorimetry. The laser induced surface damage threshold for the grown crystal was determined using Nd:YAG laser. The Kurtz powder second harmonic generation efficiency of grown LPSBT is about 0.8 times that of potassium dihydrogen orthophosphate.

**Keywords:** *Growth from solution, X – ray diffraction, Laser damage threshold, Photoluminescence, Second harmonic generation.*

\*Corresponding author  
Dr. S. Sathiskumar  
Assistant Professor  
Department of Physics  
Shri Angalamman College of Engineering and Technology  
Tiruchirappalli – 620 105, Tamil Nadu, India  
Tel.: +91 – 7708502466  
E – Mail address: [sathisphy@rediffmail.com](mailto:sathisphy@rediffmail.com), [sathiskumarmphy@gmail.com](mailto:sathiskumarmphy@gmail.com)

## 1. Introduction

Nonlinear optical materials for second harmonic generation (SHG) efficiency have received consistent attention for applications in the field of telecommunication, optical computing, optical information processing, optical disk data storage, laser remote sensing, laser driven fusion and colour displays. Amino acid ligands coordinated with metals display specific features of interest like molecular chirality, acentric crystallographic structures, absence of strongly conjugated bonds leading to high transparency range in the UV - visible spectral region and zwitterionic nature of molecules favour the crystals hardness [1, 2]. Proline is a rigid amino acid and is exemplified by the fact that it is one of the largest components of the protein collagen, the main protein that forms connective tissue in humans and other higher organism [3]. L – proline a well known interesting material for nonlinear optical (NLO) applications as it contains a proton donor carboxyl group ( $\text{COO}^-$ ) and the proton acceptor amino group ( $\text{NH}_3^+$ ). L – proline has been proved to combine with alkali halides, alkali earth and transition metal halogenides coordination compounds such as cadmium, lithium, mercury, zinc, strontium and manganese [4 - 9]. In the course of our search for new noncentrosymmetric compounds our group synthesized L – proline strontium bromide tetrahydrate (LPSBT) and the three dimensional crystal structures was recently published by us [10]. In the present investigation we report the growth of the bulk crystal of L – proline strontium bromide tetrahydrate and its structural, morphological, optical, thermal,

dielectric, etching studies, photoluminescence, laser damage threshold, mechanical and nonlinear optical properties for the first time.

## 2. Experimental Section

### 2.1 Synthesis

L – proline strontium bromide tetrahydrate (LPSBT) was synthesized by reacting equimolar quantities of L – proline and strontium bromide tetrahydrate in double distilled water at room temperature. Scheme 1 represents the reaction mechanism for the formation of the LPSBT compound. Calculated amount of strontium bromide tetrahydrate was first dissolved in double distilled water. L – proline was then added to the solution slowly by continuous stirring using a temperature controlled magnetic stirrer. The solvent was allowed to evaporate at room temperature and the salt was obtained. The recrystallization process was carried out thrice to improve the purity of the synthesized salt.

### 2.2 Solubility

To grow bulk single crystals from solution by slow evaporation technique, a suitable solvent is to be selected in which the solute has to dissolve moderately. The size of a growing crystal depends on the amount of solute available in the solution, which in turn is decided the level of solubility of the material in that particular solvent. To determine the equilibrium concentration, aqua solution of LPSBT was prepared using double distilled water. The solution was maintained at a constant temperature and continuously stirred using a magnetic stirrer to ensure identical temperature and concentration throughout the volume of the solution. On getting the saturation, the concentration of the solute was analyzed gravimetrically. The same procedure was repeated for each temperature. The temperature dependence of solubility of LPSBT is shown in Fig. 1. From the graph, it is observed that the solubility of LPSBT increases with increase of temperature.

### 2.3 Crystal growth

L – proline strontium bromide tetrahydrate single crystal was grown from aqueous solution by slow evaporation solution growth technique at room temperature. The saturated solution was prepared from recrystallized salt at room temperature and was then filtered to remove any unsolvable impurities. The solution was covered with perforate polythene sheet and then housed in a dust free atmosphere to allow solvent evaporation. After a growth period of 15 days colourless single crystals of size  $1.5 \times 0.8 \times 0.7$  cm<sup>3</sup> were harvested and are shown in Fig. 2. The morphology of LPSBT crystal is a polyhedron and the crystallographic planes (01 $\bar{1}$ ), (100), (011), (01 $\bar{1}$ ), (0 $\bar{1}$ 0), (001), (0 $\bar{1}$ 1) and ( $\bar{1}$ 00) are identified from XRD studies. Figure 3 shows the morphology and the crystallographic planes of the as grown LPSBT single crystal.

## 3 Results and discussion

### 3.1 Single crystal X – ray diffraction analysis

Single crystal X – ray diffraction analysis was carried out using Bruker Nonius CAD 4 diffractometer equipped with a CCD detector and graphite monochromated Mo K $\alpha$  radiation ( $\lambda = 0.71703$  Å) at 296 K. A transparent crystal with dimensions  $0.15 \times 0.1 \times 0.1$  mm<sup>3</sup> was mounted on a thin glass fiber with epoxy for X – ray diffraction. The structure was solved by direct methods and then refined by a full-matrix least-squares refinement on F<sup>2</sup> with the computer program SHELXL – 97 as programmed in the software suite WinGX v 1.64.03. Crystal data and refinement summaries are given in Table 1. The crystallographic information file has been deposited by us in the Cambridge structure data base (CCDC No: 1424731) and can be obtained free of charge from the Cambridge Crystallographic Data Centre via [www.ccdc.cam.ac.uk/data\\_request/cif](http://www.ccdc.cam.ac.uk/data_request/cif). As shown in the ORTEP diagram (Fig. 4),

the asymmetric unit contains a proline molecule, one Sr cation, four Br<sup>-</sup> anions and four water molecules.

### **3.2 Powder X – ray diffraction analysis**

The grown single crystal was subjected to powder X – ray diffraction studies using BRUKER X – ray diffractometer with Cu K $\alpha$  ( $\lambda = 1.5407 \text{ \AA}$ ) radiation. The sample was scanned in the range of 10 - 80° at the rate of 2° /min. The obtained d values are indexed using AUTOX 93 software package. The indexed powder XRD pattern is shown in Fig. 5.

### **3.3 Fourier transform infrared and FT - Raman spectral analysis**

Fourier transform infrared (FT – IR) spectral analysis was carried out using Perkin Elmer FTIR spectrometer by KBr pellet technique in the range of 400 – 4000 cm<sup>-1</sup>. The FT – Raman spectrum was obtained using Bruker RFS 27 FT – Raman spectrometer in the range of 50 – 4000 cm<sup>-1</sup>. The recorded FTIR and FT – Raman spectrum are shown in Fig. 6 and Fig. 7 respectively. The small strong band at 3491 cm<sup>-1</sup> in IR and 3446 cm<sup>-1</sup> in Raman are assigned to the OH stretching vibration. The bands at 3057 cm<sup>-1</sup> and 3013 cm<sup>-1</sup> in FTIR are due to N – H asymmetric and symmetric stretching vibrations respectively. The band at 2885 cm<sup>-1</sup> in Raman, 2727 cm<sup>-1</sup> in FT – IR is attributed to the C – H stretching vibration. The strong IR band at 1600 cm<sup>-1</sup> and Raman band at 1633 cm<sup>-1</sup> indicate the existence of the COO<sup>-</sup> ion in zwitterionic form. The frequency observed at 1418 cm<sup>-1</sup> is due to the COO<sup>-</sup> symmetric stretching vibration. The FT – IR vibration modes observed at 1368 cm<sup>-1</sup> and 1344 cm<sup>-1</sup> are assigned to CH<sub>2</sub> wagging and twisting vibration respectively. The medium intensity FT – IR band at 1094 cm<sup>-1</sup> and 984 cm<sup>-1</sup> is assigned to the CH<sub>2</sub> rocking and C – C – N stretching mode of vibrations respectively. The band observed at 856 cm<sup>-1</sup> in Raman spectrum for CH<sub>2</sub> rocking mode of vibration. The vibration observed at 782 cm<sup>-1</sup> in FT – IR and the peak observed at 780 cm<sup>-1</sup> in Raman is assigned to the COO<sup>-</sup> in plane deformation. The peak

observed at 532 cm<sup>-1</sup> is assigned to Br<sup>-</sup> in plane deformation. The observed wavenumbers are compared with L – proline strontium chloride monohydrate in Table. 2.

### 3.4 UV – Vis – NIR spectral analyses

The optical transmittance spectrum was recorded using a Perkin Elmer Lambda 35 spectrophotometer in the wavelength range 190 – 1100 nm. The recorded transmittance and absorption spectrum of grown LPSBT crystal is shown in Fig. 8. The crystal exhibits moderate transmittance and the lower cut off wavelength is observed at 240 nm. In the case of metal organic coordination complexes, group (IIB) metals are extensively chosen as their compounds show a high precision in the UV region because of their filled d<sup>10</sup> shell [11]. High transmittance in the visible and near IR region with lower cut off wavelength is the most favorable characteristics of a prospective candidate for NLO applications [12]. The optical absorption coefficient ( $\alpha$ ) was calculated from the transmittance spectrum using the relation  $\alpha = 2.3036 \log (1/T)/d$ , where T is the transmittance and d is the thickness of the crystal. The direct optical band gap energy (E<sub>g</sub>) of LPSBT was estimated using the relation  $\alpha = A (hv - E_g)^{1/2}$  / hv, where h is the Planck's constant and A is a constant. The Tauc plot drawn between  $(\alpha hv)^2$  and photon energy (eV) is shown in Fig. 9. The band gap was evaluated by the extrapolation of the linear part with X - axis. The band gap of LPSBT is ~5.2 eV.

### 3.5 Photoluminescence study

The photoluminescence (PL) emission spectrum of LPSBT crystal was recorded by using a HORIBA Scientific spectrofluorometer with 450 W high pressure xenon lamp. The PL intensity is dependent on the crystallinity and structural perfection of the grown crystal. LPSBT crystal was excited at wavelength of 300 nm. As shown in Fig. 10, a weak luminescence emission peak is observed at 425 nm and it is assigned to intraligand  $\pi - \pi^*$  transition of the carboxylate ion [13]. The PL intensity is gradually reduced in the higher wavelength due to the presence of electron donating group NH<sub>3</sub><sup>+</sup> and electron withdrawing

group of  $\text{COO}^-$  that can augment the mobility of  $\pi$  electrons [14]. The broadening of emission band is due to inter molecular interactions. The energy at this peak was calculated using the formula  $E_g = hc/\lambda$ . Here  $h$  is the Planck's constant,  $c$  is the velocity of light and  $\lambda$  is the wavelength of luminescence. The calculated band gap energy is 3.4 eV, which corresponds to this PL emission peak. The peak observed at 425 nm indicates that the crystal has blue emission.

### 3.6 Vickers microhardness

Mechanical strength of LPSBT crystal was estimated by using Vickers microhardness tester at room temperature. Crystal of dimensions  $10 \text{ mm} \times 8 \text{ mm} \times 5 \text{ mm}$  with a flat and smooth (001) plane was chosen for stagnant indentation test and it was mounted on the base of the microscope controlled by XY travel stage. Loads varying from 1 to 100 g were indented for a dwell period of 10s using Vickers diamond pyramid indenter. Length of the two diagonals was measured by a calibrated micrometer attached to the eyepiece of the microscope after unloading and the average length of the diagonals was found out. Two indentations were considered for a particular load and the average of diagonals ( $d$ ) was in use for the hardness value ( $H_v$ ) calculation. Hardness number was estimated using the standard formula  $H_v = 1.8544 (P/d^2) (\text{kg}/\text{mm}^3)$  where  $P$  is the applied load in kg,  $d$  is the indentation impression in mm. Figure 11 shows the variation of hardness number as a function of applied load for LPSBT single crystal. It is obvious from the Fig. 11 that the hardness value increases with increase in the load. The load above 100 g develops multiple cracks on the crystal surface due to the discharge of internal stresses generated locally by indentation. Meyer's index was calculated from  $P = Kd^n$ , which relates the applied load and indentation diagonal length ( $d$ ).  $\log P = \log k + n \log d$ , where  $k$  is the material constant and  $n$  is the Meyer's index.

The Meyer's relation indicates that  $H_v$  should increase with  $P$ , if  $n > 2$  and decrease with  $P$  when  $n < 2$ . In order to find the value of  $n$ , a graph is plotted for  $\log P$  versus  $\log d$  (Fig. 12) which gives a straight line. From the slope, Meyer's index  $n$  was calculated and found to be 2.3. According to Hanneman [15] the value of  $n$  lies between 1 and 1.6 for hard materials, where as the values of  $n$  greater than 1.6 indicate the softer ones. Thus the present result shows that the LPSBT belongs to softer once.

### 3.7 Dielectric studies

Optical quality single crystal of LPSBT was selected for the dielectric measurement studies using HIOKI 3520 – 50 LCR HITESTER in the frequency range from 50 Hz to 2 MHz at a variety of temperatures. Silver paste was applied on each faces to make a capacitor with the grown crystal as a dielectric medium. The crystal was sited between two copper electrodes, which act as a parallel plate capacitor. The capacitance of the material was measured at dissimilar frequencies from 50 Hz to 2 MHz. The dielectric constant was calculated using the relation  $\epsilon_r = Cd / (\epsilon_0 A)$ , where  $C$  is the capacitance,  $d$  is the thickness of the crystal,  $\epsilon_0$  is the permittivity of free space and  $A$  is the area of the crystal. Variation in the dielectric constant versus log frequency is shown in Fig. 13. The value of dielectric constant is higher in the lower frequency region and then decreases with increase in the applied frequency. The high value of dielectric constant at lower frequencies may be due to the presence of all the four polarizations namely space charge, orientation, electronic and ionic polarizations and its lower value at higher frequency may be due to considerable loss in the polarizations. From the Fig. 13, it is also observed that there is no noticeable variation in the values of dielectric constant with respect to temperature.

The dielectric loss was calculated using the relation  $\epsilon'' = \epsilon_r D$ , where  $D$  is the dissipation factor. The variation of dielectric loss versus log frequency is depicted in Fig. 14. From the graph, it is found that the dielectric loss decreases with increase in frequencies. The

value of dielectric loss is higher at lower frequencies and it is lower at higher frequency region. The low values of dielectric loss entail that the crystal possesses enhanced optical quality with lesser defects and these parameters indicate that the material can be appropriate for NLO applications [16].

### **3.8 Thermal analyses**

#### **3.8.1 Thermogravimetric analysis**

Thermogravimetric analysis (TGA) was carried out using Perkin Elmer STA 6000 thermal analyzer between room temperature to 1400 °C in nitrogen atmosphere at a heating rate of 10 °C/min. The recorded TGA curve of LPSBT is shown in Fig. 15. There are three major steps in the weight loss. The first step of weight loss is observed between the temperature range 60 and 210 °C. This step of weight loss indicates the taking away of four water molecules present in the crystal lattice. The second stage of weight loss occurs between the temperature range of 280 and 493 °C. This step of weight loss is due to the removal of proline molecule. The third step of weight loss starts at the temperature 920 °C and ends at 1400 °C. On further heating the grown crystal up to 1400 °C the materials gets reduced to anhydrous strontium bromide.

#### **3.8.2 Differential Scanning Calorimetry analysis**

Differential Scanning Calorimetry (DSC) analysis was carried out on a NETZSCH STA 409C instrument with a heating rate of 10 °C/min. A small piece of a crystal weighing 12.287 mg was placed in an aluminium pan. The recorded DSC plot is shown in Fig. 16. The DSC plot shows a phase transition at 130 °C. The well noticeable exothermic peak is due to the loss of four water molecule. The second endothermic peak obtained at about 377 °C is ascribed to the removal of proline molecule. Finally the broad exothermic peak is observed at 1031 °C. This exothermic peak is point out, which may be the starting of weight loss for strontium bromide molecule.

### **3.9 Scanning Electron Microscopy analysis**

The scanning electron microscopy (SEM) study gives information about the nature of surface morphology in the grown crystals. The morphology of the grown crystal surface was observed by a scanning electron microscopy (SEM) using a JSM 253 SEM analyzer. The obtained micrographs of the LPSBT crystal scanned at two different magnifications 2.66 kx and 779x are shown in Fig. 17a and 17b respectively. From the illustration of 779x magnification, it is observed that the surface consists of regular morphological habits of the arrangement of atoms (Fig. 17a) thus showing a perfect growth surface with a few microcrystallites on the surface.

### **3.10 Energy Dispersive X - ray analysis**

Energy dispersive X – ray analysis (EDAX) was carried out and it offers information about the elemental composition of the grown LPSBT single crystal. The grown LPSBT crystal was subjected to EDAX using a JSM 253 SEM analyzer with Genesis Eds software to confirm the presence of strontium and bromine radicals in the grown crystal. Figure 18 illustrates the EDAX spectrum of LPSBT single crystal, which confirms the occurrence of carbon, nitrogen, oxygen, strontium and bromine in the grown crystal. The percentage of various elements present in the LPSBT single crystal is given in the Table 3.

### **3.11 Chemical etching studies**

The chemical etching studies were carried out on the grown LPSBT crystal using double distilled water as an etchant at room temperature for the etching period of 5s and 10s. The etch patterns were observed using an optical microscope in the reflection mode fitted with high resolution Motic camera. The crystal was completely immersed into the distilled water for 5s. The surface of the crystal was examined carefully at many places. Fig. 19a shows the formation of rectangular and circular etch pits on the surface of the grown crystal

for etching time of 5s. Etching the surface further fresh surface behind it can be seen. This is confirmed from the Fig. 19b which shows the etch pits grow in size, the probability that new smaller etch pits are initiated inside it. This leads to a self feeding process in which the etch pits become larger. Thus when the etching time was increased there is no change in the etch pattern but there is an increase in the size of the etch pits.

### **3.12 Nonlinear optical property**

The Kurtz and Perry [17] powder technique is a valuable tool for initial screening of materials for second harmonic generation (SHG). The crystal was crushed into a harmonized powder of micro crystallites and compactly packed in a capillary of identical bore and is kept in a cell holder. The powder SHG measurement was carried out for LPSBT with fundamental 1064 nm laser beam radiation. A Quanta Ray (Model LAB – 170 – 10) of Nd: YAG laser producing pulse with a width of 8 ns and a repetition rate of 10 Hz was used. The incident light energy 0.7 J was used to strike the powder crystalline sample. The second harmonic signals from the sample were paying attention into a Czerny – Turner monochromator using a pair of lenses. The SHG signal was established by the emission of green radiation (532 nm) and the optical signal was collected by a photomultiplier tube (PMT). The output signal was displayed on the oscilloscope (CRO). The SHG efficiency estimated is 0.8 times that of the reference the standard KDP sample. Comparison of second harmonic generation signal efficiency of LPSBT crystal along with other amino acid based nonlinear optical crystals with respect to potassium dihydrogen orthophosphate crystal is presented in Table 4.

### **3.13 Laser damage threshold**

The applications of nonlinear optical crystals depends not only on the linear and nonlinear optical properties but also largely on its potential to survive high power laser. The bulk materials appear more damage resistant than the crystal surfaces. For that reason the presentation of the grown crystal mainly depends on surface quality. Laser damage value of

LPSBT crystal was measured using Q – switched Nd:YAG laser operating in transverse mode ( $\text{TM}_{00}$ ). Pulse width of 10 ns with a repetition rate of 10 Hz and fundamental wavelength of 1064 nm was used for this experiment. Laser induced breakdown of materials is caused by a multiplicity of physical mechanism. For visible materials, the damage is due to avalanche and multi photon ionizations. The damage threshold in the case of strong absorbing materials is due to the increasing of temperature, which creates strain – induced fracture. The laser damage energy density of LPSBT crystal was bringing into being  $1.01 \text{ GW/cm}^2$ .

#### **4. Conclusion**

A new metal organic single crystal of L – proline strontium bromide tetrahydrate was effectively synthesized and single crystals were grown by slow evaporation technique at room temperature. LPSBT crystallizes in orthorhombic system with the noncentrosymmetric space group of  $\text{P}2_1\text{2}_1\text{2}_1$ . Various crystallographic planes are well-known by X – ray diffraction studies. The presences of functional groups were established by FT – IR and FT – Raman spectral studies. Optical studies confirm that LPSBT crystals can be used for optical window applications in the wavelength range of 240 – 1100 nm. The microhardness measurement shows that the hardness value of LPSBT single crystal is increases with increase in the applied load (P) and the grown crystal clearly tells about reverse indentation size effect. The Meyer's index number (n) was calculated for the grown crystal and shows that it belongs to soft materials category. The dielectric constant and dielectric loss studies establish the normal dielectric behaviour for LPSBT single crystal. Thermogravimetric analysis reveals that the material decomposition at three stages due to evaporation of constituents graphs. Photoluminescence spectrum shows blue emission in the grown LPSBT crystal and the strong charge transfer occurs in the molecules. The SEM images of LPSBT showed the shape in circular tubules structure on the surface of the crystal. The percentage of elements present in the crystal was known using EDAX analysis, which confirms the

presence of various elements. Etching studies tell the formation of circular and rectangular etch patterns. The laser damage threshold of the grown LPSBT crystal is  $1.01 \text{ GW/cm}^2$ . The second harmonic generation efficiency of the crystal is 0.8 times that of KDP.

## References

- [1] D. S. Chemla, J. Zyss, Nonlinear optical properties of organic molecules and crystals, Vol. 1, Academic Press, Orlando, 1987.
- [2] G. Venkatesan, G. Anandha Babu, P. Ramasamy, A. Chandramohan, J. Molecular structure 1033 (2013) 121 – 126.
- [3] S. E. McLain, A. K. Soper, A. E. Terry, A. Watts, J. Phys. Chem. B 111 (2007) 4568 – 4580.
- [4] A. Kandasamy, R. Siddeswaran, P. Murugakoothan, P. Suresh Kumar, R. Mohan, Cryst. Growth Des., 7 (2007) 183 – 186.
- [5] S. Sathiskumar, T. Balakrishnan, K. Ramamurthi, S. Thamotharan, Spectrochim. Acta Part A 138, 2015, 187 – 194.
- [6] D. Kalaiselvi, R. Jayavel, Appl. Phys. A 107 (2012) 93 – 100.
- [7] G. Anandha Babu, P. Ramasamy, Mater., Chem. Phys. 113 (2009) 727 – 733.
- [8] K. Manoj Gupta, Nidhi Sinha, Binay Kumar, Physica B 406 (2011) 63 – 67.
- [9] Z. Rzaczynska, R. Mrozek, T. Glowik, J. Chem. Crystallogr. 27 (1997) 417 – 422.
- [10] S. Sathiskumar, T. Balakrishnan, K. Ramamurthi, S. Thamotharan, Acta Cryst. E71 (2015) 1199 – 1202.
- [11] M. H. Jiang, Q. Fang, Adv. Mater. 11 (1999) 1147
- [12] J. Mary Linet, S. Dinakaran, S. Jerome Das, J. Alloys Comp. 509 (2011) 3832
- [13] F. F. Li, J. F. Ma, S.Y. Song, J. Yang, Cryst. Growth Des., 6 (2006) 209 – 215.  
S. R. Fan, L. G. Zhu, J. Inorg. Chem. 45 (2007) 7935 – 7942.
- [14] Z. Deng, F. Bai, Y. Xing, N. Xing, L. Xu, Open J. Inorg. Chem. 3 (2013) 76 – 99.

- [15] M. Hanneman, Metall. Manchu 23 (1941) 135
- [16] M. Briget Mary, M. Uma Devi, S. Pandiarajan, V. Ramakrishnan, Spectrochim. Acta Part A 60 (2004) 2643 – 2651.
- [17] S. K. Kurtz and T. T. Perry, J. Appl. Phys. 39, 1968, 3798 – 3813.

**Scheme Caption****Scheme 1 Reaction mechanism of LPSBT****Figure Caption****Fig. 1 Solubility curve of LPSBT****Fig. 2 As grown single crystals of LPSBT****Fig. 3 Various crystallographic planes of the as grown LPSBT single crystal****Fig. 4 ORTEP diagram of LPSBT****Fig. 5 Powder X – ray diffraction pattern of LPSBT****Fig. 6 FT – IR spectrum of LPSBT crystal****Fig. 7 FT – Raman spectrum of LPSBT crystal****Fig. 8 UV – Vis – NIR transmittance and absorption spectrum of LPSBT****Fig. 9 Photon energy versus  $(\alpha h\nu)^2$  of LPSBT crystal****Fig. 10 Photoluminescence spectrum of LPSBT****Fig. 11 Mechanical behaviour of LPSBT****Fig. 12 Meyers plot of LPSBT****Fig. 13 Variation of log f versus dielectric constant of LPSBT****Fig. 14 Variation of log f versus dielectric loss of LPSBT****Fig. 15 TGA of LPSBT single crystal****Fig. 16 DSC curve of LPSBT****Fig. 17 (a) SEM micrograph of LPSBT crystal****Fig. 17 (b) SEM micrograph of LPSBT crystal****Fig. 18 EDAX spectrum of LPSBT single crystal****Fig. 19 (a) Etch patterns on LPSBT crystal for 5s****Fig. 19 (b) Etch patterns on LPSBT crystal for 10s**

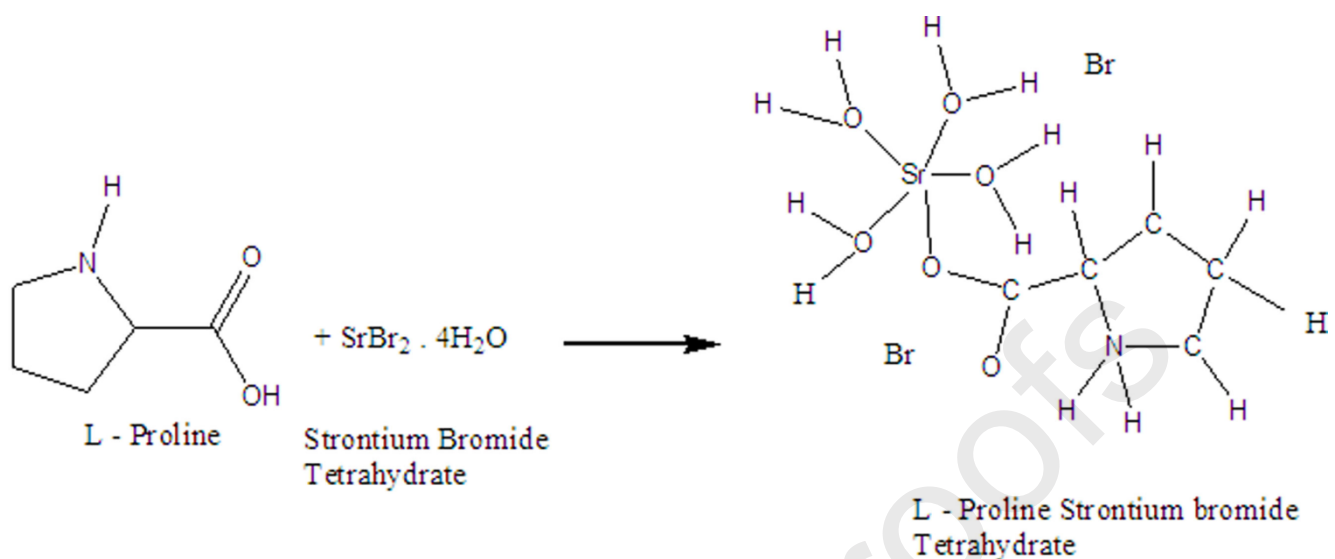
**Table Caption**

**Table 1 Crystal data and structure refinement details for LPSBT**

**Table 2 Infrared and Raman spectral band assignments of LPSBT**

**Table 3 Compositional analysis of LPSBT crystal from EDAX spectra**

**Table 4 Comparative SHG efficiency of different semiorganic NLO crystals relative to KDP crystal**

**Scheme 1**

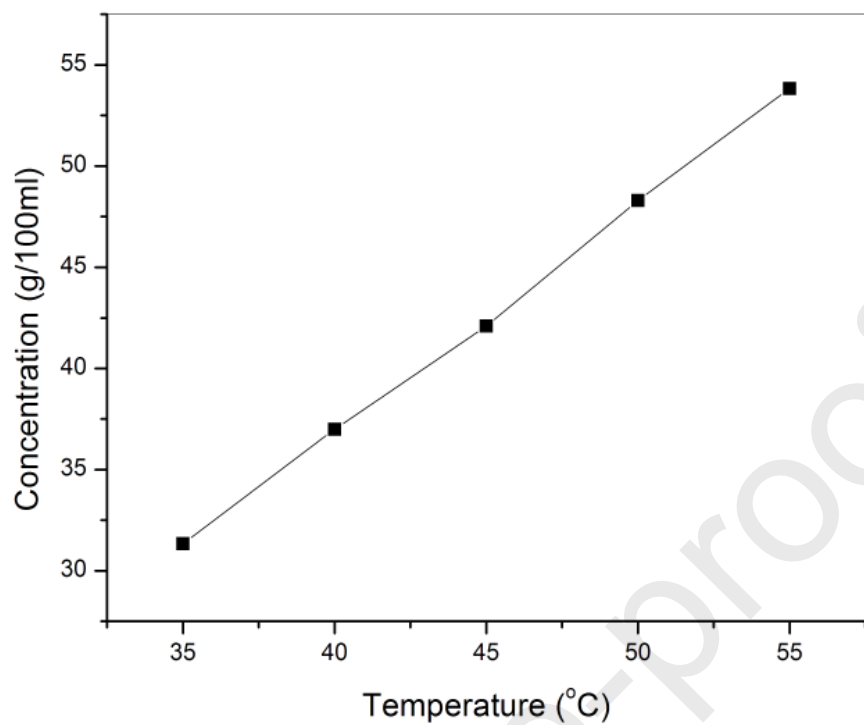
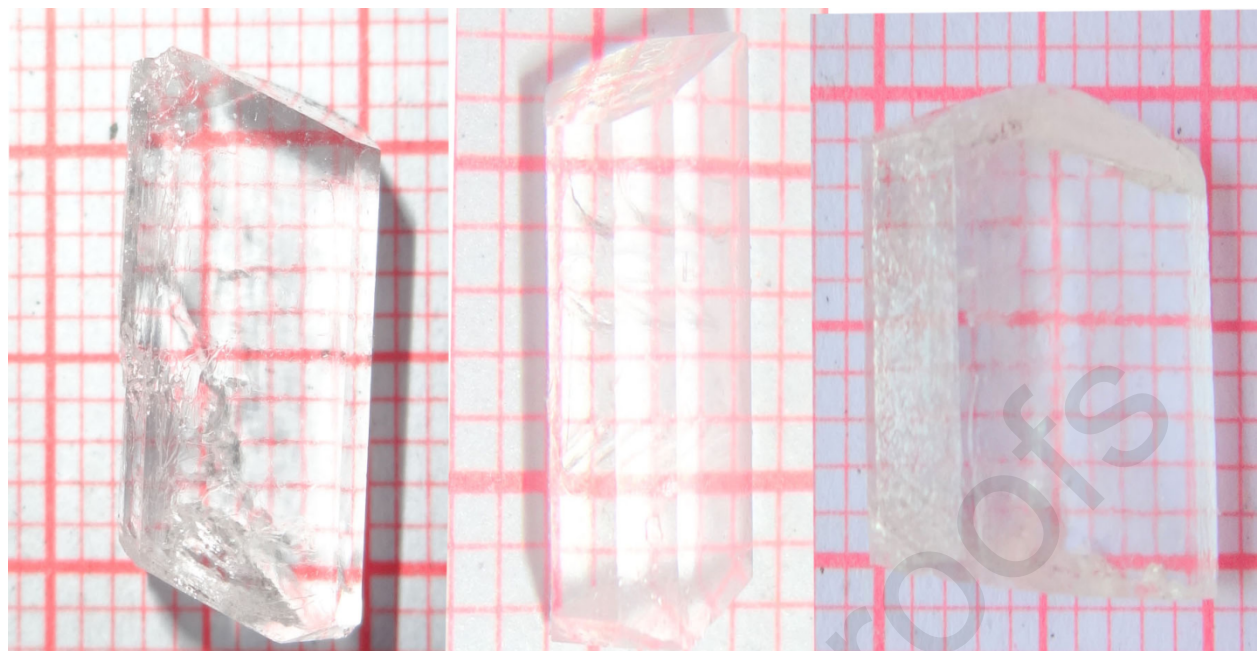


Fig. 1



**Fig. 2**

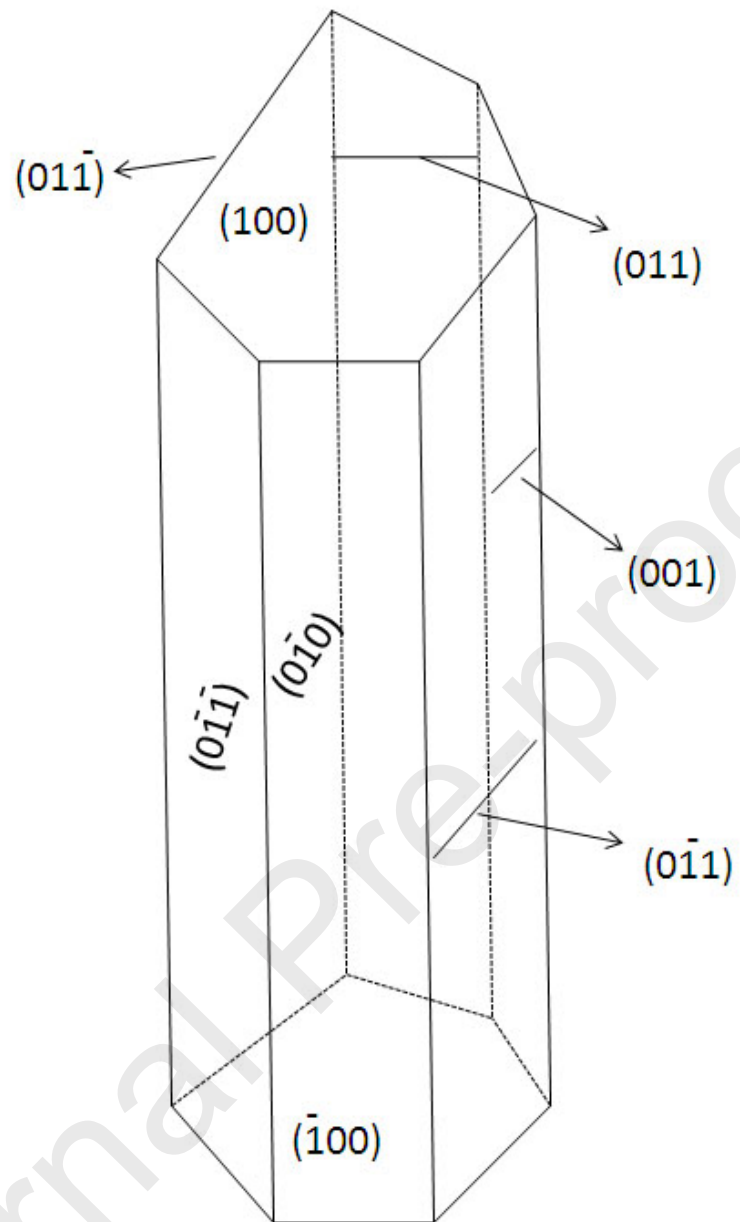


Fig. 3

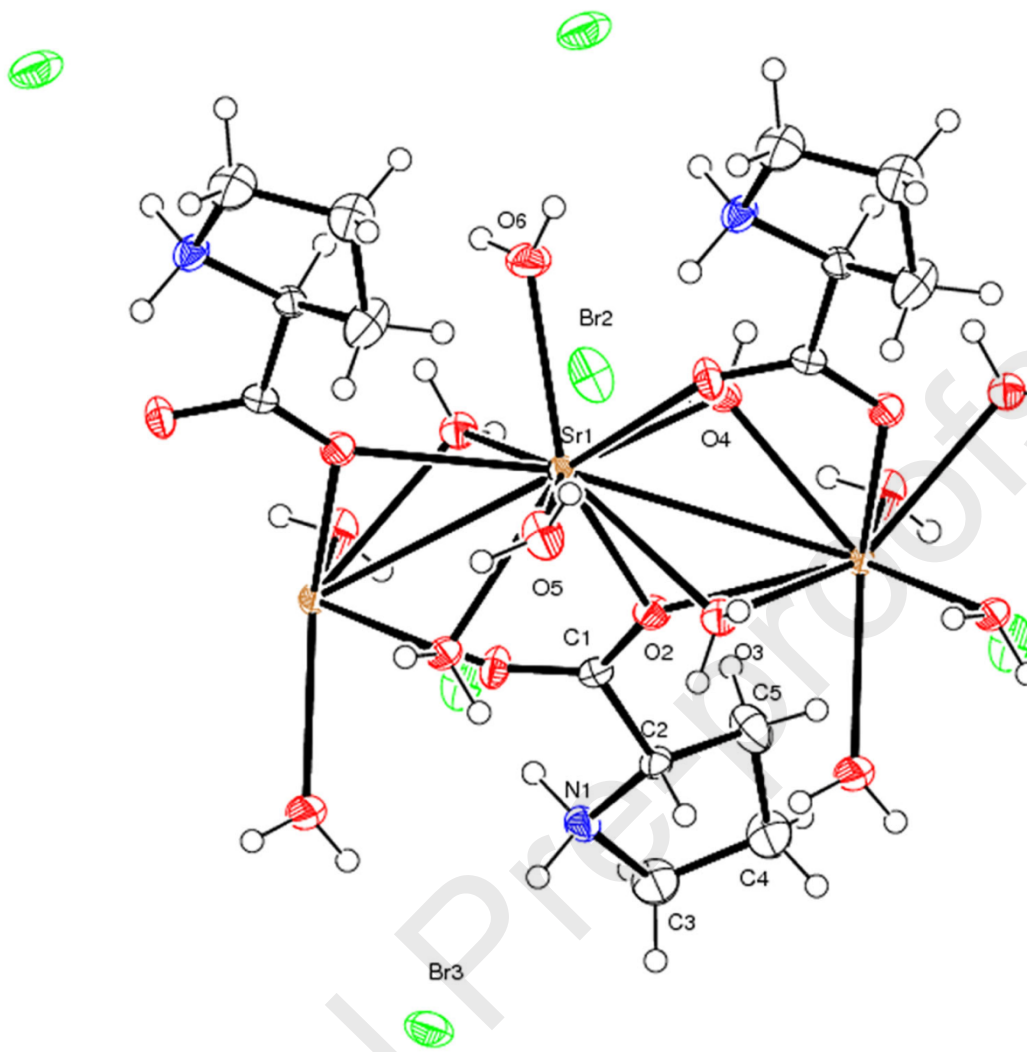


Fig. 4

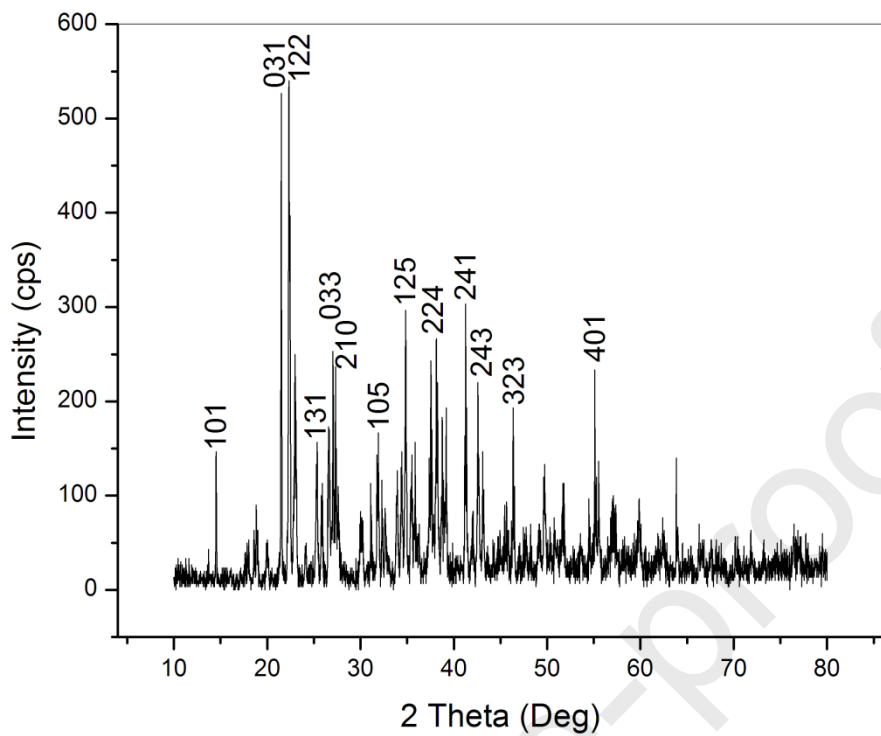


Fig. 5

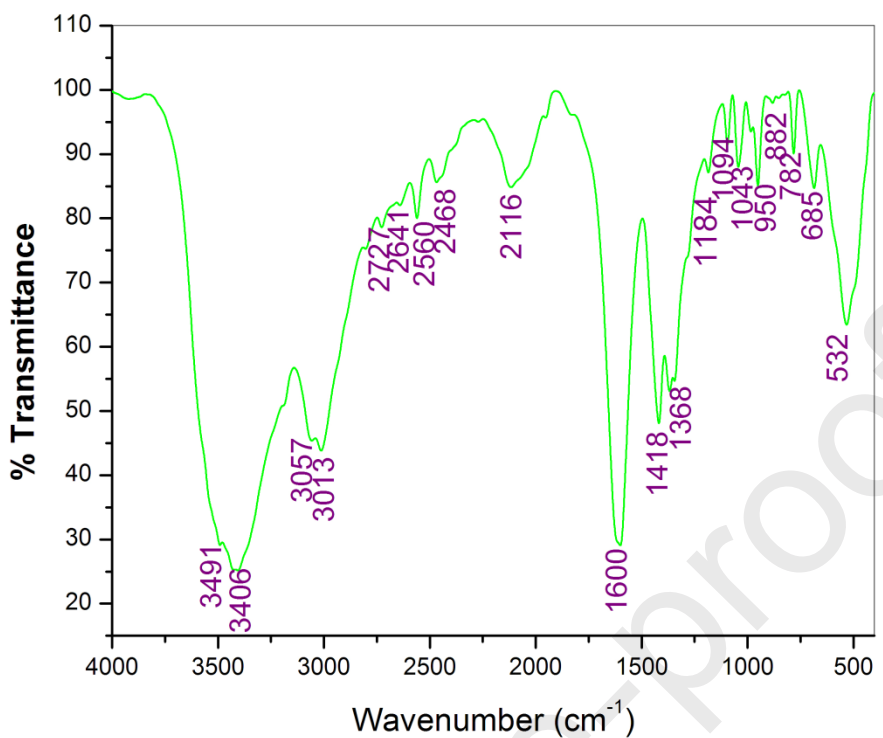


Fig. 6

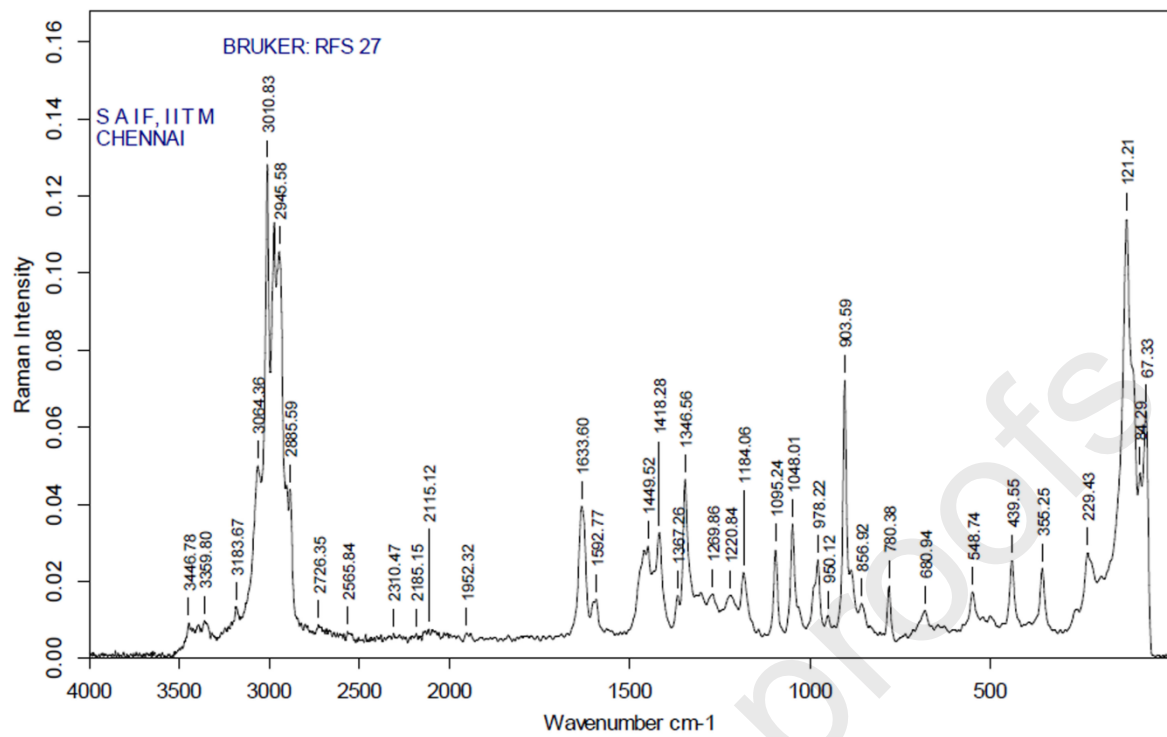


Fig. 7

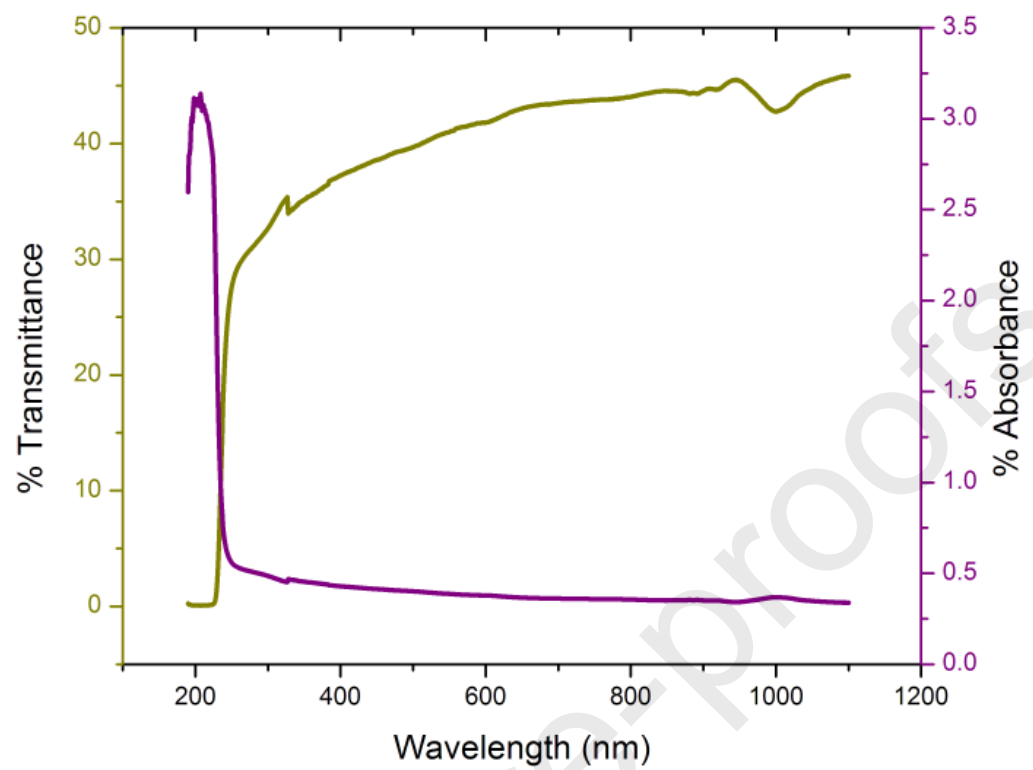


Fig. 8

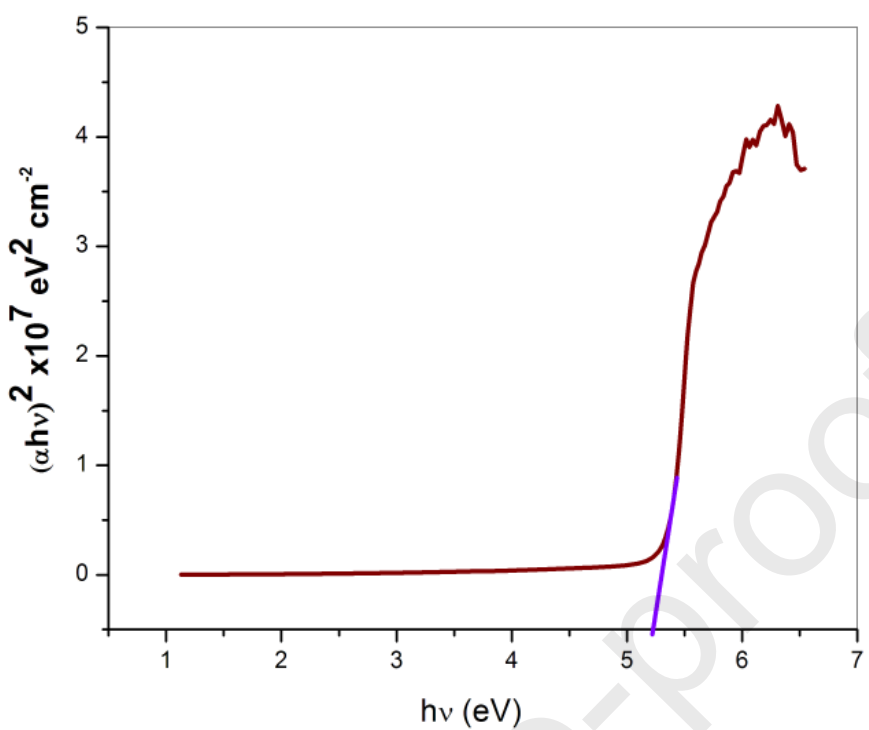


Fig. 9

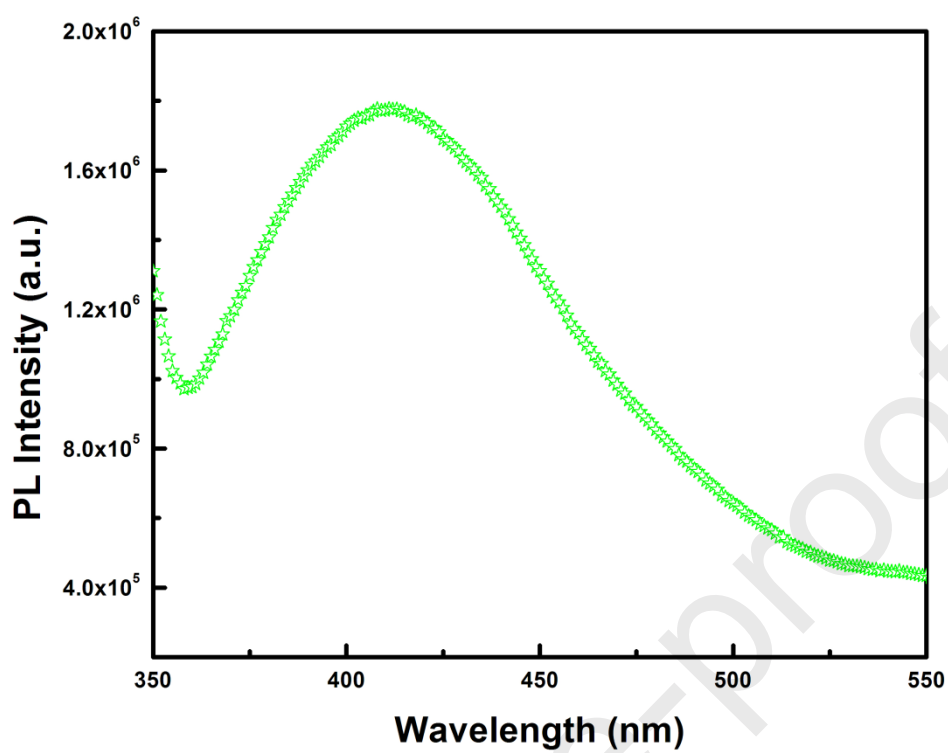


Fig. 10

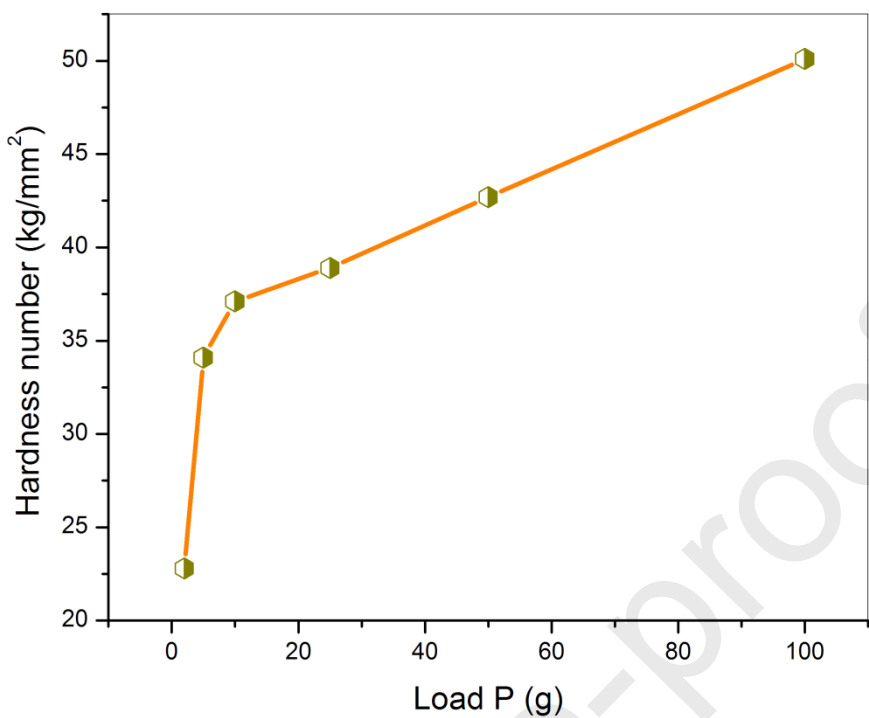


Fig. 11

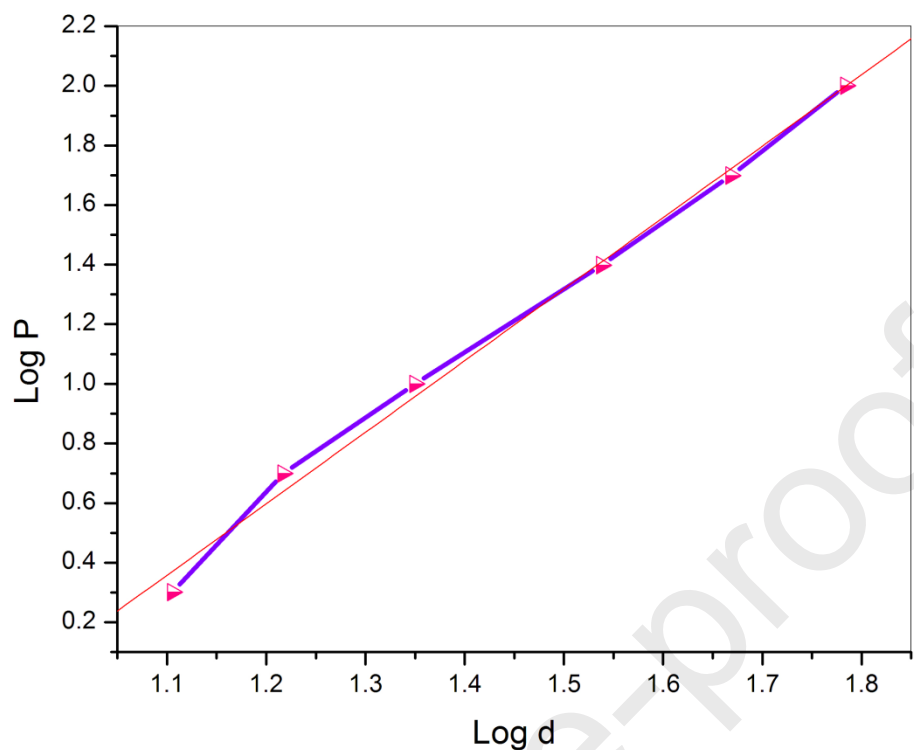


Fig. 12

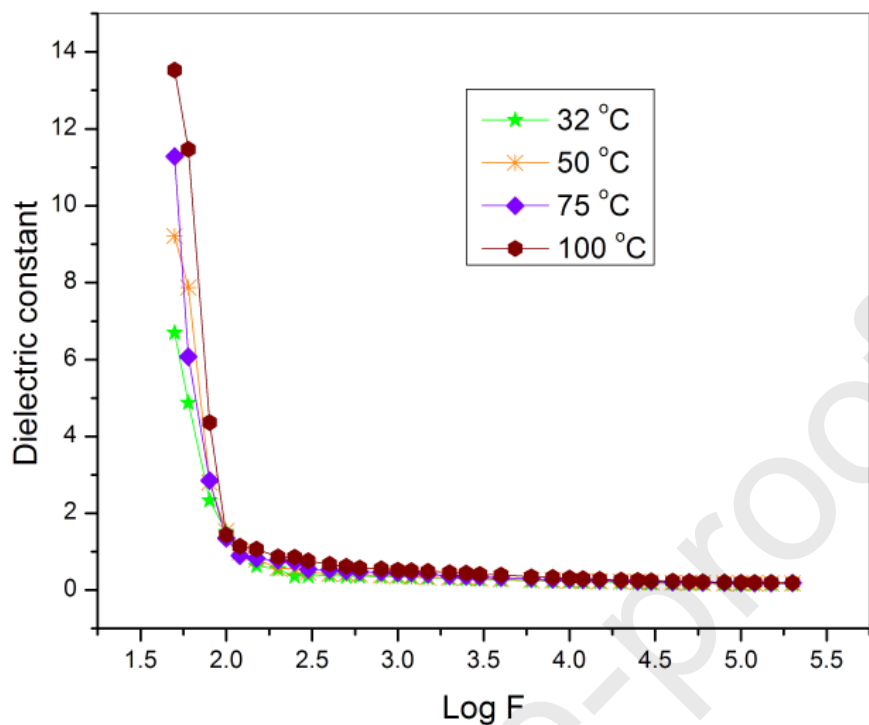


Fig. 13

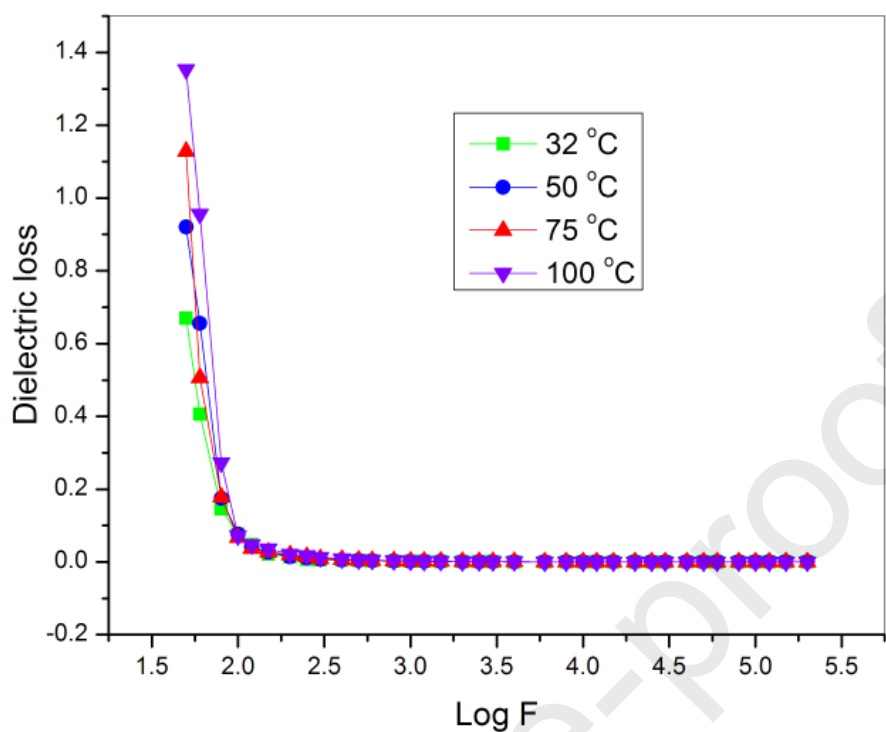


Fig. 14

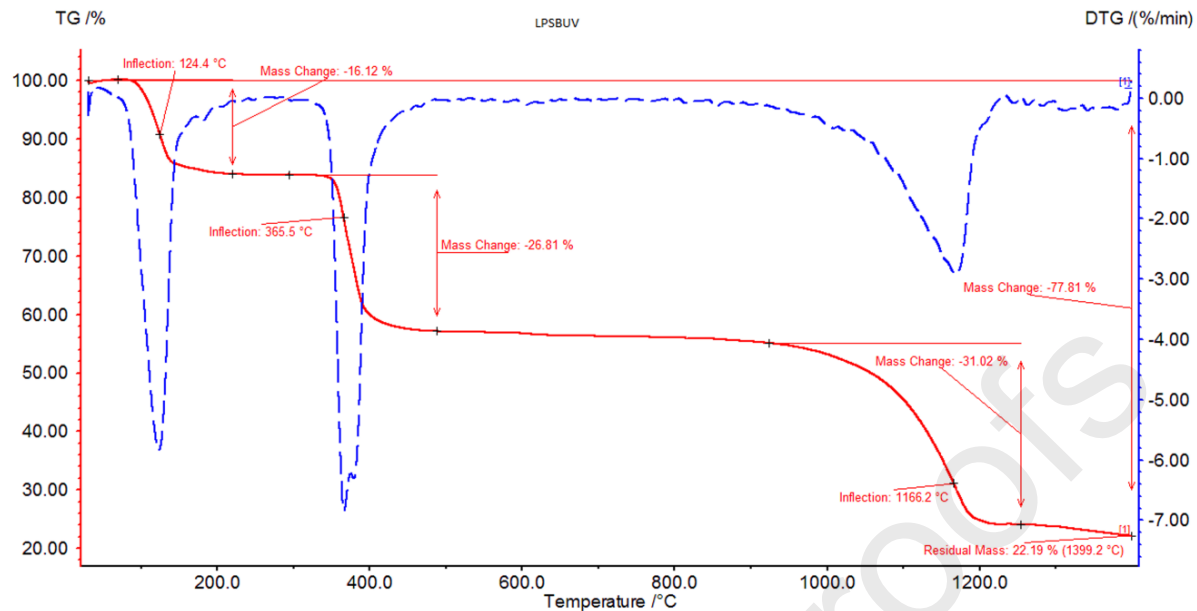


Fig. 15

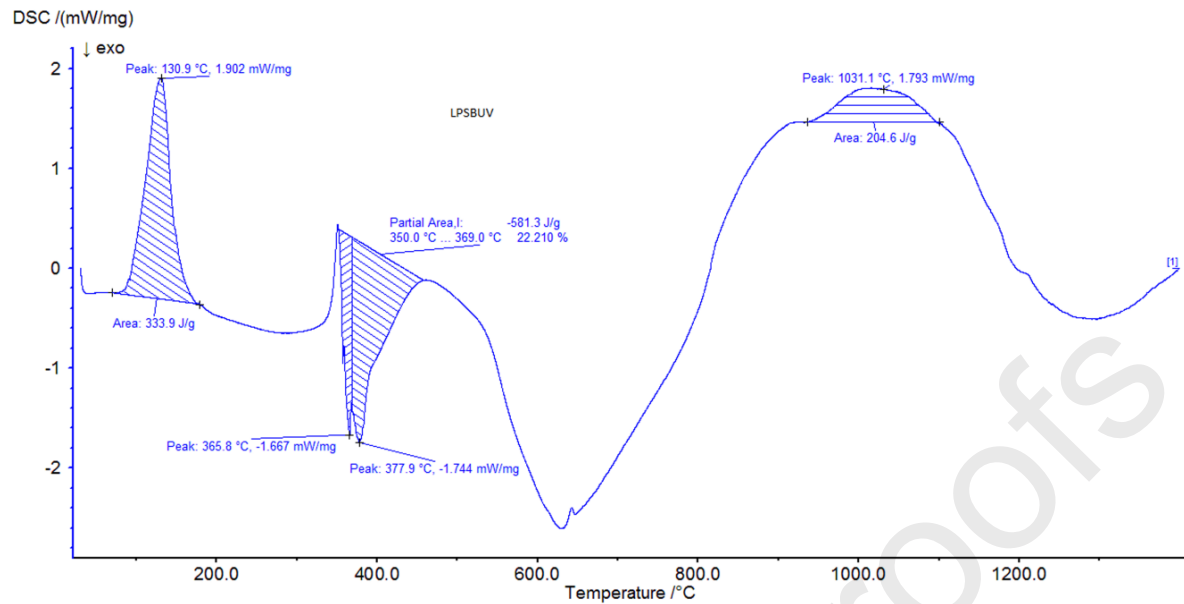
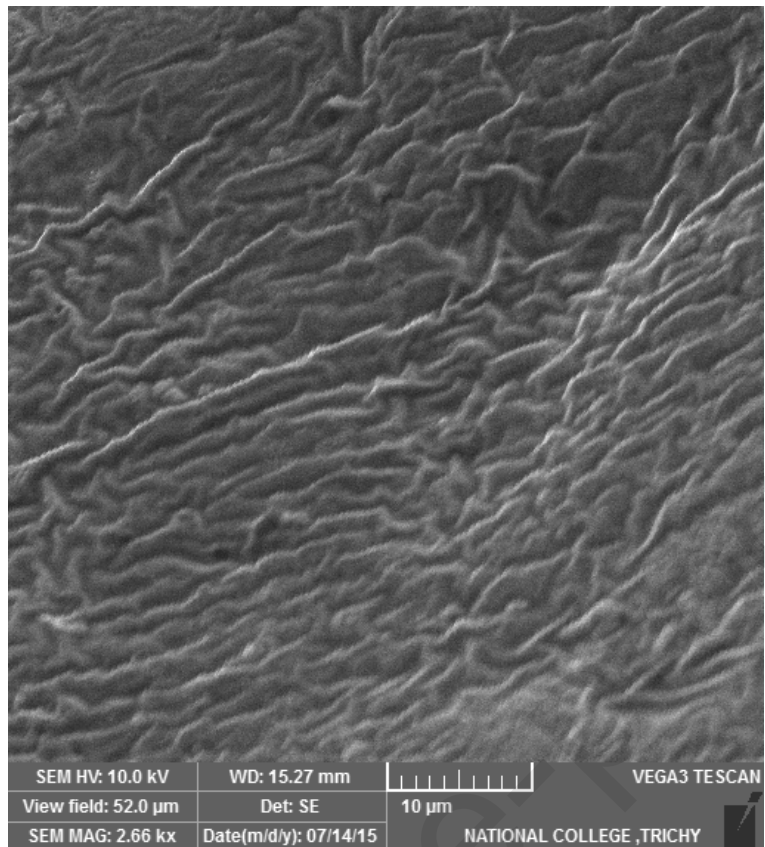
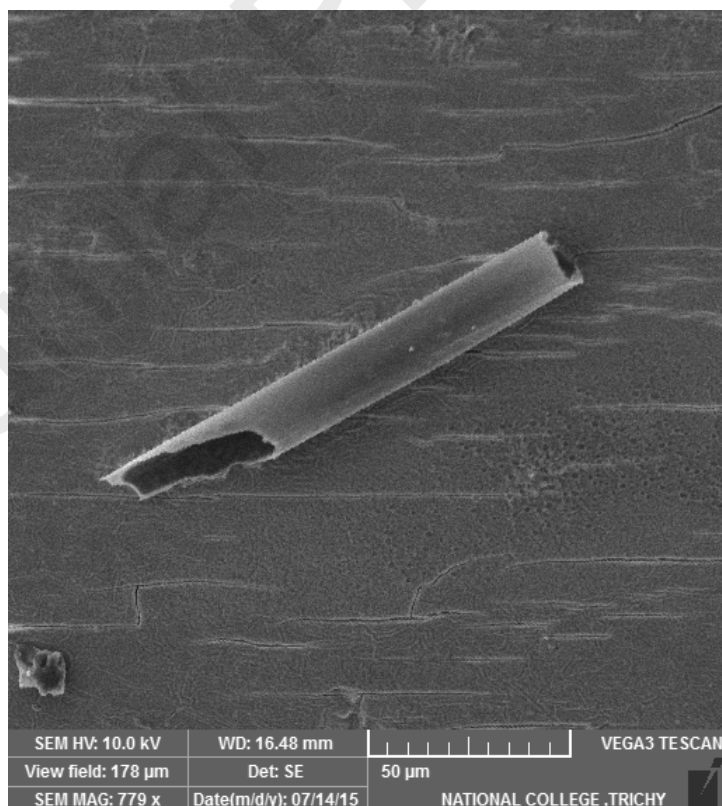


Fig. 16



**Fig. 17 (a)**



**Fig. 17 (b)**

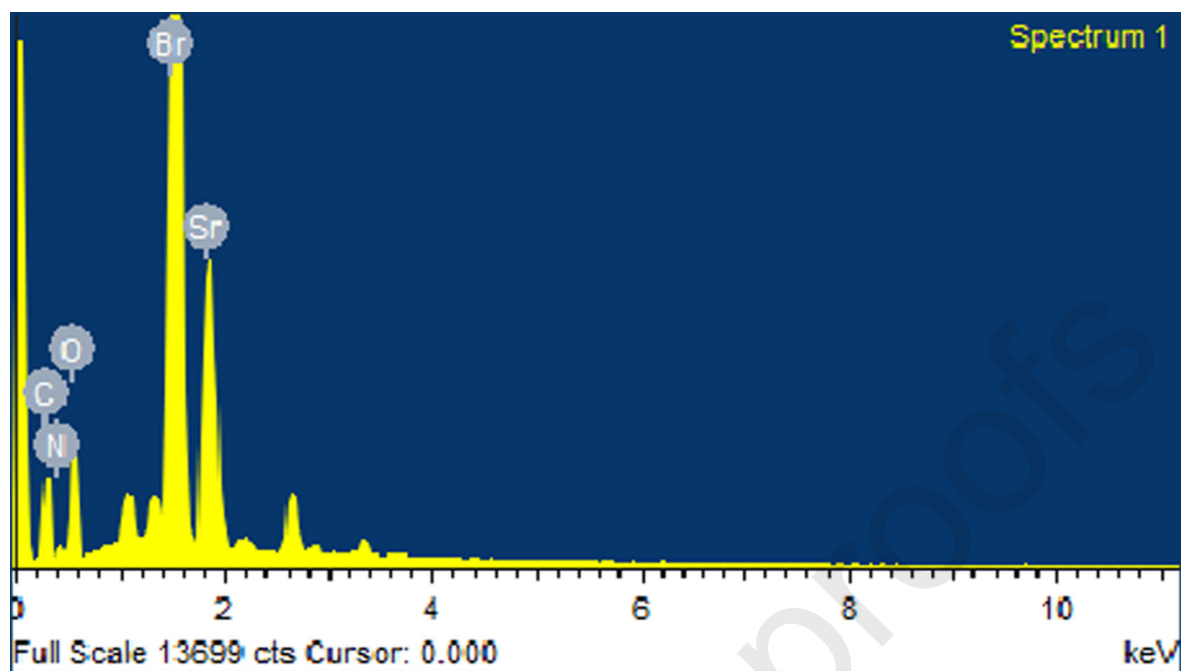
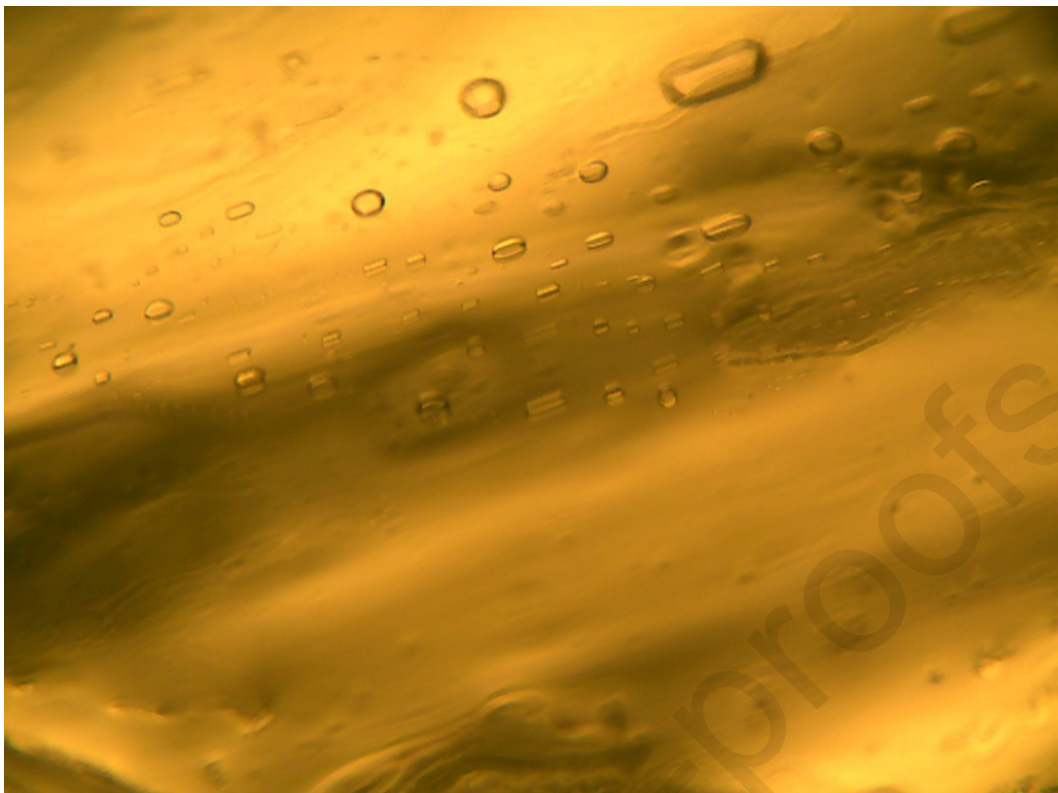
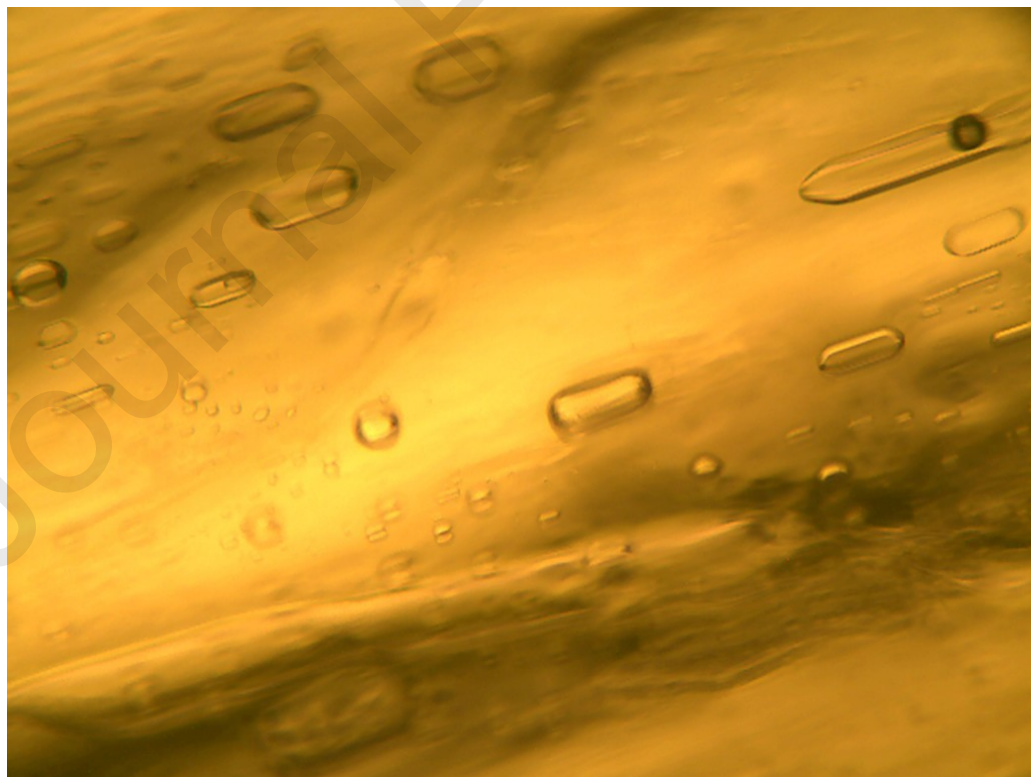


Fig. 18



**Fig. 19 (a)**



**Fig. 19 (b)**

**Table 1**

<b>Crystal Data</b>	
Formula	C <sub>5</sub> H <sub>17</sub> Br <sub>2</sub> · Sr NO <sub>6</sub>
Formula weight	434.63 g/mol
Crystal color, habit	Colorless, plate
Crystal system	Orthorhombic
Crystal size	0.15 × 0.10 × 0.10 mm <sup>3</sup>
Space group	P2 <sub>1</sub> 2 <sub>1</sub> 2 <sub>1</sub>
Z, Calculated density	4, 2.157 Mg/m <sup>3</sup>
Unit cell dimensions	a = 6.7079 (4) Å    α = 90° b = 12.9125 (9) Å    β = 90° c = 15.4499 (11) Å    γ = 90°
Volume	1338.20 (16) Å <sup>3</sup>
F (000)	840

**Table 2**

LPSBT		LPSCM [8]	Band assignments
FT – Raman	FT - IR	FT - IR	
3446	3491	-	Stretching vibration of H <sub>2</sub> O
3064	3057	-	NH asymmetric stretching
3010	3013	-	NH symmetric stretching
2945	-	-	NH <sub>3</sub> <sup>+</sup> symmetric stretching
2885	2727	-	CH stretching
1633	1600	1628	C=O asymmetric stretching
1592	-	-	NH <sub>2</sub> <sup>+</sup> in – plane deformation
1449	-	-	CH <sub>2</sub> bending
1418	1418	1419	COO <sup>-</sup> symmetric stretching
1367	1368	1369	CH <sub>2</sub> wagging
1346	1344	1334	CH <sub>2</sub> twisting
1269	-	-	C – O stretching
1184	1184	-	NH <sub>2</sub> <sup>+</sup> twisting
1095	1094	1100	CH <sub>2</sub> <sup>+</sup> rocking
1048	1043	1045	C – N stretching
978	984	-	C – C – N stretching
950	950	954	NH <sub>2</sub> <sup>+</sup> rocking
-	882	-	C – C stretching
856	-	-	CH <sub>2</sub> rocking
780	782	-	COO <sup>-</sup> in – plane deformation
680	685	691	COO <sup>-</sup> wagging
439	532	-	Br <sup>-</sup> in plane deformation

**Table 3**

<b>Element</b>	<b>Weight %</b>	<b>Atomic %</b>
C	27.47	49.89
N	7.18	11.18
O	19.71	26.87
Sr	16.50	4.11
Br	29.13	7.95
Total	100.00	100.00

**Table 4**

<b>Nonlinear optical crystals</b>	<b>SHG efficiency</b>
L – Proline strontium bromide tetrahydrate (Present study)	0.8
L – Proline trichloroacetate	0.5
L – Proline strontium chloride monohydrate	0.08
L – Proline lithium chloride monohydrate	0.2
Di-bromide L – Proline zinc	0.5
L – Phenylalaninium trichloroacetate	0.65
L – Arginine chloride	0.2
L – Arginine bromide	0.3
L – Alanine	0.2
L – Valinium succinate	0.56